INSTITUTE OF PHYSICS PUBLISHING NANOTECHNOLOGY
Nanotechnology **13** (2002) 644–652 PII: S0957-4484(02)35105-5

Fabrication by means of x-ray lithography of two-dimensional GaAs/AlGaAs photonic crystals with an unconventional unit cell

F Romanato[1], L Businaro[1], E Di Fabrizio[1], A Passaseo[2], M De Vittorio[2], R Cingolani[2], M Patrini[3], M Galli[3], D Bajoni[3], L C Andreani[3], F Giacometti[4], M Gentili[4], D Peyrade[5] and Y Chen[5]

[1] NNL (National Nanotechnology Laboratory), TASC-INFM @ ELETTRA Synchrothron Light Source-S.S14 Km 163.5, 34012 Basovizza, Trieste, Italy
[2] NNL (National Nanotecnology Laboratory), INFM, Università di Lecce, via per Arnesano, I-73100 Lecce, Italy
[3] INFM and Dipartimento di Fisica 'A Volta', Università di Pavia, Via Bassi 6, I-27100 Pavia, Italy
[4] Pirelli Labs Optical Innovation (c.2152), Viale Sarca, 222, 20126 Milano, Italy
[5] CNRS–LPN, Route de Nozay, 91460 Marcoussis, France

Received 20 March 2002, in final form 7 August 2002
Published 16 September 2002
Online at stacks.iop.org/Nano/13/644

Abstract
Two-dimensional photonic crystals have been fabricated by x-ray lithography and reactive ion etching on an air/GaAs/AlGaAs asymmetric waveguide. The shape of the lattice unit cell has been varied by exploiting x-ray diffraction effects and nonlinear response of resists during the development process. Rings with or without a central pillar have been fabricated with a resolution down to 50 nm. Lithographic details are described to show the accuracy of this fabrication technique. Optical characterization has been performed showing the presence of a well defined photonic band structure as well as band anti-crossing. The results are discussed and compared with theoretical calculations of the photonic band dispersion. Structures with high dielectric fraction are shown to yield photonic modes with small line widths and low propagation losses. The reliability and the precise control of the fabricated sample structures make this lithographic method useful for a full investigation of optical properties on the dependence of the lattice unit cell shape.

(Some figures in this article are in colour only in the electronic version)

1. Introduction

Photonic crystals (PCs) represent one of the most important building blocks towards the achievement of a full based optics communication technology. Even though straightforward application of the photonic bandgap (PBG) concept is generally thought to require a three-dimensional PC [1–4], the largest interest so far is attracted by two-dimensional PCs because they are potentially more amenable to fabrication and much closer to application [5]. However, definite standardization is still far from being achieved and different fabrication methods [6–8], architectures and integration strategies [9–11] of two-dimensional PCs are under investigation and in competition to produce the first target to market devices.

In this framework, among fundamental issues definitively cleared, many open questions still remain. For instance the dependence of two-dimensional PC optical characteristics on the shape of the unit cell is not still well explored.

This is a problem that has been largely investigated in the early pioneering theoretical works [12, 13] with the aim to indicate the lattice structure that can produce a full PBG. When several groups then conclusively showed that a triangular array of air columns gives rise to a large and complete PBG [14, 15], the relevance of the unit cell shape dependence was almost forgotten leaving some muddled questions unsolved. Fabrication complications to effectively control the unit cell shape at sub-micrometric accuracy have further set the unit cell dependence issue aside. Some of these issues have been only recently re-addressed, enlightening the complexity of phenomenology. Theoretical investigations on the optimization of the PBG as a function of the symmetry, shapes and orientations of the unit cell base have shown that a reduction of the degree of symmetry can increase the PBG [16]. The symmetry of the unit cell moreover can influence the light propagation. In particular elliptical deformation of the unit cell base structures in two-dimensional PCs with a square lattice has been experimentally demonstrated by Noda *et al* [17] to be the key feature to control the propagation of polarization. To our knowledge no further experiments have been performed to investigate this issue. One of the reasons can be addressed to the challenging technological problem of controlling the fabrication of the unit cell shape with lateral resolution down to a few nanometres on defect free large areas.

In this work we have investigated the possibility of fabricating two-dimensional PCs with an unconventional unit cell by x-ray lithography. X-ray proximity lithography is known to provide a one-to-one replica of the features patterned on the mask [18]. This is a deceptively simple description of the image formation in x-ray lithography. A high spatial coherent illumination of the mask can induce diffraction effects that propagate along the distance between the mask and target substrate, i.e. along the mask–substrate gap. Actually lithographic images much more complex than those patterned on the mask can be generated. We will show that when full control of diffraction and of the exposed resist development is achieved, controlled and complex lithographic structures, a few nanometres wide, can be fabricated.

The technique allows the generation of an unconventional unit cell lattice starting from a relatively simple mask. In our case we have used a single x-ray mask made of a square on a square lattice. Controlling the mask–substrate gap several different types of pattern can be generated: smoothed squares, rings, rhombs or four-leaf clovers. However, in this preliminary study we focused on two-dimensional PCs constituted by lattice unit cells with ring or anti-ring shape with or without concentric pillars or holes fabricated on air/GaAs/$Al_xGa_{1-x}As$ ($x = 0.25$). In particular we have increased the lithographic lateral resolution of the structures replicated on large areas, obtaining ring widths below 50 nm. Optical characterization of the resulting PC will be presented and discussed on the basis of theoretical simulation. The dielectric filling factor of the lattice has been varied in order to investigate one of the most interesting parameters that determines the optical characteristics of PCs. Further applications and limits of this fabrication method will be discussed as well.

2. Fabrication

2.1. X-ray lithography

The proximity x-ray lithography was performed at the LILIT [19, 20] beam line located at Elettra Synchrotron (Trieste). A schematic representation of the main optical and mechanical constituents of the beam line is shown in figure 1.

The beam line consists of one plane mirror (mirror 1) placed at 14 m from the bending magnet source and of a second toroidal mirror (mirror 2) placed 2 m away from mirror 1. Both mirrors are gold-coated with an average surface roughness of 0.5 nm. The total length of the beam line, calculated from the front-end port of the bending magnet, is 13.3 m. Entry slits select the solid angle under which the synchrotron radiation is collected, fixing the maximum values at 6 and 0.83 mrad (3σ) respectively in the horizontal and the vertical plane. The latter value corresponds to the natural divergence of the synchrotron radiation in the soft x-ray range under the standard operating condition of the beam line. Just after the bending magnet front-end, a 25 μm thick beryllium window separates the vacuum between beam line and synchrotron ring. Additional energy filters are located before mirror 1. Further adjustable slits for final beam shaping are placed after mirror 2 close to the end of the beam line where, after a photon shutter and a second 25 μm thick beryllium window, the x-ray beam is delivered in a helium flux at atmospheric pressure. Both the mirrors operate at grazing angles (θ_1, θ_2) producing an image of the source at the wafer/mask location whose size is 3×50 mm^2 (vertical by horizontal). Whereas the value of θ_1 can be freely chosen in the range from 0.3° to 2.8°, the amplitude of θ_2 and the height of second mirror are, in contrast, determined by the constraints imposed by the fixed height from the ground of the source and of the final beam spot [21].

LILIT beam line is designed for performing both soft and hard x-ray lithography. Whereas hard x-rays are required for deep lithography, in this work we are mainly interested in a soft energy spectrum (1–2 keV) that is well indicated for the best lithographic resolution. The energy spectrum provided by the bending magnet of Elettra is quite wide, extending from a few hundred eV to 15 keV (see the inset in figure 1, spectrum delivered by bending magnet). The sequence of the energy spectra along the beam line shows how the effects of the different optical elements allow us to select the optimum energy spectrum (see the other spectra in figure 1 inset). In general the rejection of the low energy part of the spectrum (100 eV–2 keV), responsible for diffraction effects in one-to-one deep x-ray lithography, is performed by a series of eight films of different materials (Be, C, Al, Cr, Si_3N_4) and thickness. These films can independently intercept the beam providing 16 combinations of different high band pass filter energy. However, the present work is focused on the diffraction effects control, requiring the maximization of the low energy part of the spectrum. For this reason we have not introduced any further filter except the two fixed beryllium windows that account for a total thickness of 50 μm and whose effect on the photon beam is reported in the second spectrum in figure 1 inset. In contrast, the rejection of the hard part of the spectrum responsible for straggling effects on the formation of the latent image in the resist is very important. The effect of a tunable high band pass filter is performed by increasing the incidence

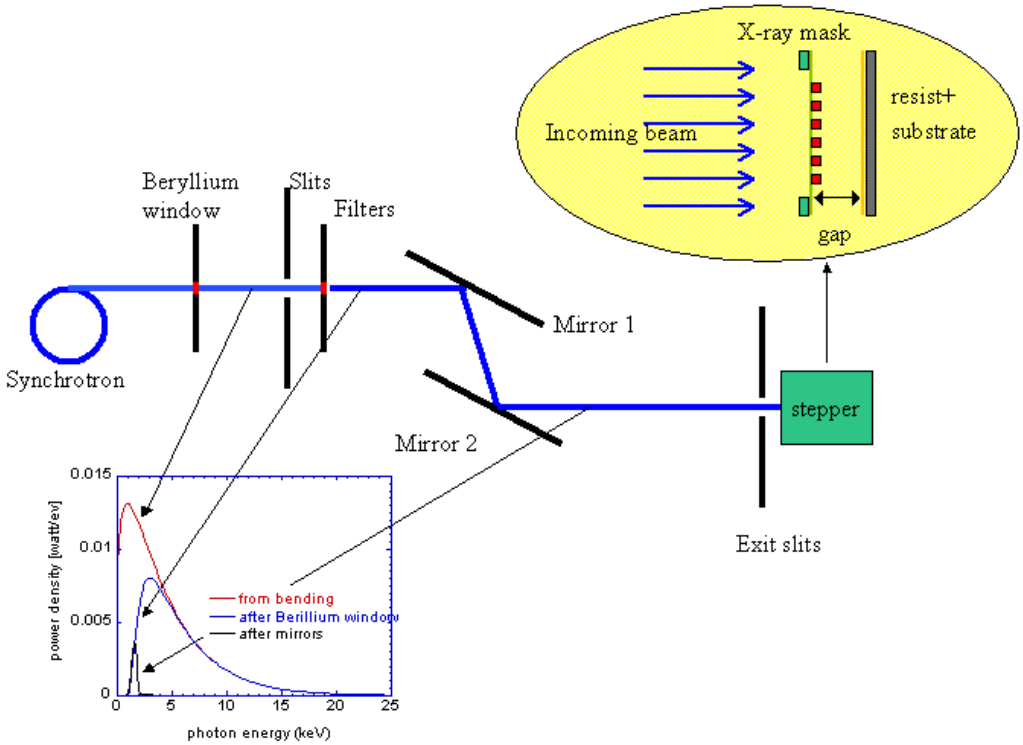

Figure 1. Scheme of LILIT beam line. The top inset shows the geometry of the x-ray mask–substrate stepper stage. The bottom inset shows the photon energy spectrum along the beam line after the main optical elements.

angle of the mirrors, that decreases the mirror reflectivity at low wavelengths. The final effect on the energy spectrum is shown on the third spectrum of the inset in figure 1 for the mirror angle configuration selected for this experiment ($\theta_1 = 2°$, $\theta_2 = 1.902°$). In general the combination of the film filters and of mirror reflectivity allows us to select the energy band pass covering a the total spectral region of the x-ray lithographic window (1.5–15 keV).

The final x-ray beam illuminates the lithographic mask that *shadows* its pattern on a resist film typically spun on a silicon 4 in wafer substrate. The alignment of the x-ray mask with respect to the resist wafer is provided by a SAL x-ray stepper that allows step and repeat x-ray exposures with an overall placement accuracy (3σ) of 20 nm. In the framework of this study the mask–substrate gap distance, g, plays a fundamental role. The SAL x-ray stepper can fully automatically drive from 50 μm down to 30 μm and, operator supported, down to 5 μm.

2.2. Mask for x-ray lithography

For this experiment we have used a mask generated by electron beam lithography on a 4×4 mm^2 area (figure 2). It consists of a chessboard lattice of squares with a period of 500 nm along the diagonals. The patterning was exposed on a 400 nm thick film of polymethylmethacrylate (PMMA) spun on a Au/Cr coated Si_3N_4 2 mm thick membrane and pre-baked at 170 °C on a hotplate. After development for 30 s in a 1:3 solution of methyl isobutyl ketone and isopropyl alcohol (MIBK:IPA) and rinsing in IPA, the patterned area was filled by electro-plating deposition with 350 nm thick of gold film. The remaining PMMA was then stripped in hot acetone at 50 °C.

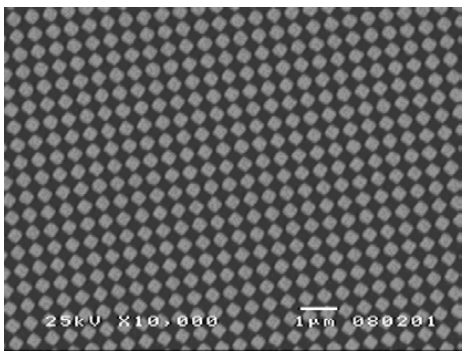

Figure 2. X-ray mask patterned with squares on a chessboard matrix of 500 nm period along the square diagonals. The markers are 1 μm long.

2.3. Sample growth and fabrication

The samples studied in this work were grown in a horizontal LP-MOCVD system (AIXTRON 200 AIX), equipped with a rotating substrate holder, at a growth pressure of 20 mbar. Trimethyl gallium (TMGa), trimethyl aluminium (TMAl) and pure arsine (AsH_3) were used as source materials and palladium purified H_2 with a flow rate of 7 slm as carrier gas. The growth was performed on (100) exactly oriented semi-insulating GaAs substrates at the nominal growth temperature of 750 °C. The structure consists of a 200 nm GaAs buffer layer, followed by 1500 nm of $Al_{0.25}Ga_{0.75}As$ and 500 nm of GaAs as topmost layer. The whole structure was grown at the rate of 4 μm h^{-1} and unintentionally doped.

The pre-exposure process steps require the cleaning in hot acetone and drying of the substrate and spinning of the resists

that we chose of both tones: PMMA 1.07 (positive), SAL 601 (negative). 150 nm of PMMA was spun on the samples and pre-baked at 170 °C on a hotplate for 5 min. In the other case SAL 601 was spun at 200 nm and pre-baked at 105 °C for 1 min. The most relevant exposure parameter was the mask–substrate gap that we selected as three values: 5, 10 and 15 μm.

The exposure doses were 2400 and 125 mJ cm^{-2} respectively for PMMA and SAL 601 samples. The latter were post-baked for 1 min at 105 °C on a hotplate. PMMA samples were developed for 45–50 s in a 1:3 solution of MIBK:IPA and rinsed in IPA. SAL 601 samples were developed for 5 min in MF312 diluted in H_2O and rinsed with de-mineralized water. The process was completed including a reactive ion etching in oxygen at 5×10^{-2} Torr and a plasma power of 50 W to guarantee a complete cleaning of the bottom of the structures.

Finally, a lift-off process was performed by evaporating 50 nm of nickel followed by the residual resist stripping. Nickel showed an extremely high selectivity to the reactive ion etching (RIE) performed by an induced coupled plasma RIE reactor in a atmosphere of 95% $SiCl_4$ and 5% of Ar and biasing the cathode at 230 V. The etching rate was 0.39 μm min^{-1} and a typical total etching time of 5 min led to an etch depth of about 2 μm in the patterned regions.

2.4. Sample description

Three samples prepared with SAL 601 resist and named S5, S10 and S15 have been exposed setting the mask–substrate gap at 1, 10 and 15 μm respectively (figures 3(a)–(c)). A fourth sample[6], P15, spun with PMMA was exposed at 15 μm mask–substrate gap (figure 3(d)). The details of the cross-sectional view of sample P15 (figure 4) selected as representative of all the other samples show that the lithographic pattern has been effectively etched along the thickness of the epitaxial AlGaAs film providing structures with aspect ratios of the order of 7. Notice in figure 4 the layering of the epitaxial growth and the residual nickel film used as a mask layer during the reactive ion etching.

What is interesting to notice is the dependence of the lattice unit cell on the mask–substrate gap distance. In the case of 5 μm mask–substrate gap (figure 3(a)) the mask features are well reproduced. This is the case of proximity x-ray lithography where a one-to-one replica of the mask can be achieved and where the diffraction effects have been almost completely suppressed by minimizing the mask–substrate gap.

The effects of the diffraction, in contrast, are evident in the samples exposed at 15 μm mask–substrate gap with both negative and positive resist (figures 3(c) and (d)). The square shape of the mask lattice unit cell becomes strongly smoothed on the corners and there appears a hole (or a pillar, depending on the tone of the resist) at the square's centre. The patterning obtained exposing the negative resist appears composed by an array of rings with remarkably thin lateral wall (<50 nm). In this case the filling factor of the resulting PC, i.e. dielectric fraction on the total unit cell area, is very low and ranges from 9% for S15 to 28% for S5. Of course an opposite patterning with a very high filling factor, 78%, can be achieved using positive (PMMA) resist (figure 3(d)), that provides a final structure composed of thin rings etched into the epitaxial multilayer.

[6] The letter of the sample names indicates the resist; the number indicates the mask–substrate gap.

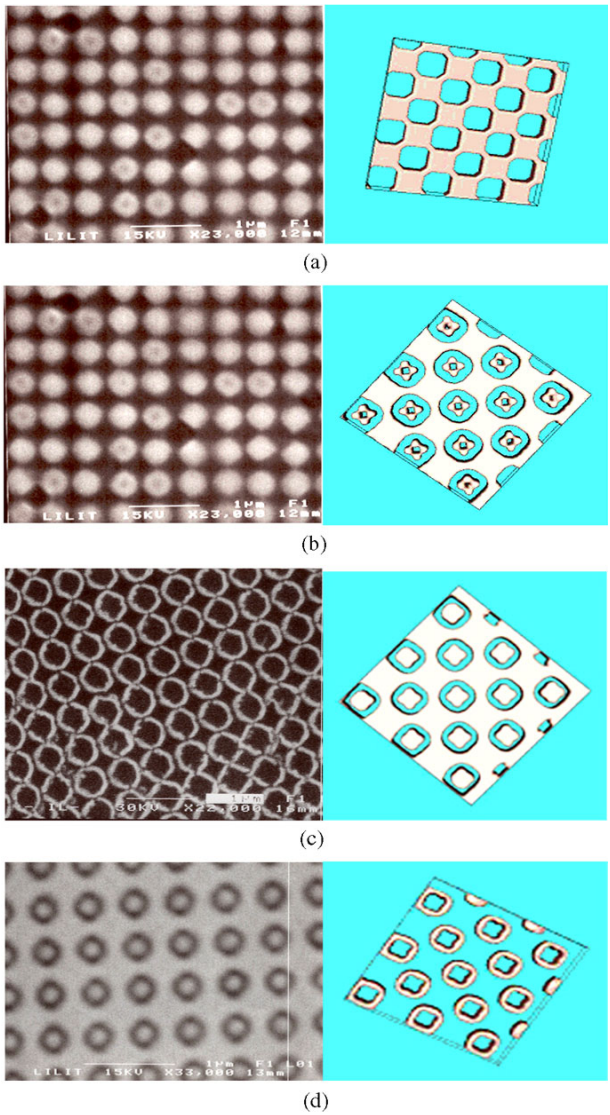

Figure 3. Pictures of the two-dimensional PC samples patterned onto air/GaAs/AlGaAs waveguide layers obtained changing the mask–substrate gap. (a) Sample S5, resist SAL601, 5 μm gap; (b) sample S10, resist SAL601, 10 μm gap; (c) sample S15, resist SAL601, 15 μm gap; (d) sample P15, resist PMMA, 15 μm gap. For every sample the relative x-ray lithography simulations performed by the TOOLSET code have been attached. The markers are 1 μm long.

An even more complex case is shown by the sample S10 exposed at 10 μm mask–substrate gap (figure 3(b)). In this case there appears a further central pillar, 100 nm in diameter and 70 nm away from the external ring whose walls are 45 nm thick. It is remarkable that these high resolution structures have been reproduced almost perfectly on a surface of 4×4 mm^2.

3. Diffraction effects on proximity lithography

Simple considerations on the role of diffraction effects on proximity lithography can be argued taking into account the diffraction pattern generated by a thin aperture. The

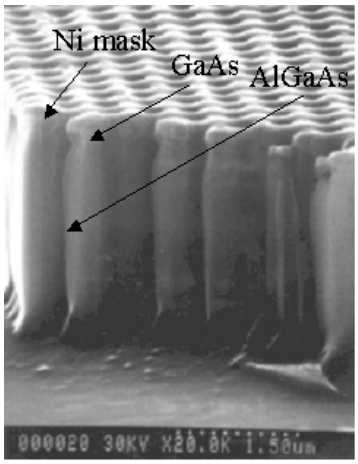

Figure 4. Lateral view of the sample showing the layering of the GaAs/AlGaAs waveguide and the residual nickel film used as a mask layer during the reactive ion etching onto the sample surface.

displacement of the first satellite peak in the diffraction pattern is given by: $\delta = g\lambda/d$. For typical values of the x-ray wavelength used in proximity lithography, $\lambda = 1$ nm, of the aperture width, $d = 200$ nm, that we identify with a typical mask feature, and of the aperture–screen distance, that in our example coincides with the mask–substrate gap $g = 15$ μm, the displacement δ turns out to be 75 nm. The linear dependence of δ on the mask–substrate gap shows that only a zero gap eliminates any diffraction effect. In our beam line the residual mask–substrate gap can be decreased down to 5 μm and it turns out that the diffraction limit to one-to-one proximity lithography is close to 25 nm. However, because a residual gap cannot be avoided it turns out that diffraction plays an important role in the one-to-one mask pattern replication, an issue that is widely discussed in the literature [22, 23].

In this work, in contrast, we exploited diffraction effects. To understand the lithographic image formation it is necessary to make some considerations on the optical characteristics of the synchrotron source we are using. In particular, due to the finite source size and the poly-chromaticity of the spectrum, the electromagnetic field responsible for the lithographic aerial image formation is partially coherent. In other words, this means that the propagation between the mask and the substrate can be rigorously calculated only using a modelling based on the theory of partial coherence. For x-ray lithography it suffices to use second order coherence theory (correlation between two wavefields at two different points in space and time coordinate) with the hypothesis that the source is homogeneous and that a modal expansion (incoherent sum of coherent modes) is used to calculate the intensity of the electromagnetic field. Under this assumption, the intensity of the electromagnetic field $I(x, y)$ can be written as the convolution between a blurring function $M(x, y)$ and the intensity $I_c(x, y)$ due to a perfectly coherent source. All the information about the coherence of the optical system is contained in $M(x, y)$. The spatial and angular blur are the parameters that take into account the degree of spatial coherence and the wavelength band pass of the light beam. The spectrum delivered by our optical system can be shaped selecting the wavelength band pass. In the case of samples described in this work, we choose to work at the minimum wavelength spread that resulted in a Gaussian spectrum centred at 0.83 nm (1.5 keV) with FWHD of 0.56 nm (700 eV). Moreover, to generate strong diffraction effects the spatial coherence of the light must be larger than the typical patterning structure dimension. From the Van Cittert–Zernike theorem, the spatial coherence length of the present beam line is

$$l_c^{\text{spatial}} = \frac{\lambda}{2\pi}\frac{L}{S} \cong 20\ \mu\text{m}$$

a value much larger than the typical patterned structures. (The beam line is characterized by a length $L = 25$ m and by a vertical bending magnet source whose size is $S = 200$ μm).

Being aware of these optical characteristics, quite untypical for a beam line devoted to x-ray lithography, we have tried to exploit the diffraction effects. The aim is to control the resulting diffraction pattern distribution to generate complex lithographic structures. This can be provided by the help of TOOLSET [24, 25], a computer code that has been specifically developed to simulate the exposure and the development of a resist in x-ray proximity lithography. In a first step the code calculates the light transmission through the different layers and near field propagation of the electromagnetic field onto the resist. Afterwards it simulates development of the exposed resist. The program requires the parameters describing the x-ray source and x-ray mask. The input parameters are therefore the natural divergence of the incoming beam, the layering of mask and its pattern, the kind of resist (thickness, chemical composition, dissolution rate), the atmosphere where the exposure takes place, the exposure and development time and finally the mask–substrate gap distance.

The latter is the parameter whose influence on the fabrication has been mainly investigated. In particular, we focused our attention on the condition for the fabrication of rings with or without central pillars generated by the squared mask (figure 2). In figure 5(a) we have reported the aerial diffraction pattern obtained for a gap of 15 μm, i.e. the gap used for samples S15 and P15 (figures 3(c) and (d)). Several peaks and dips whose position and intensity are strongly dependent on the geometrical configuration of the lattice appear. The diffraction pattern intensity along a cutting line of the mask squares has been also reported. It is worthwhile to note the single strong minimum of the centre of the transmitted beam that is responsible for the hole in the lattice unit base in figure 3(c).

In order to show the previously discussed effect of the x-ray beam coherence, in figure 5(b) we have reported for comparison the diffraction pattern obtained increasing the blur of the beam from 1 to 10 nm. In the latter case we noticed a strong decrease of the intensity modulation of the illumination pattern. The evolution of the diffraction pattern along the same cut lines simulated for different values of the mask–substrate gaps and for 1 nm blur is reported in figure 6, showing the appearance and the development of several diffraction maxima and minima. The single strong minimum of the centre of the transmitted beam for 15 μm gap and the small secondary peak for 9 μm gap are responsible respectively for the hole in the sample in figure 5(a) and for the central pillar in the sample in figure 3(b).

The diffraction is not the only effect that must be controlled to achieve the final lithographic pattern. In order to correctly develop the exposed resist an accurate optimization of the

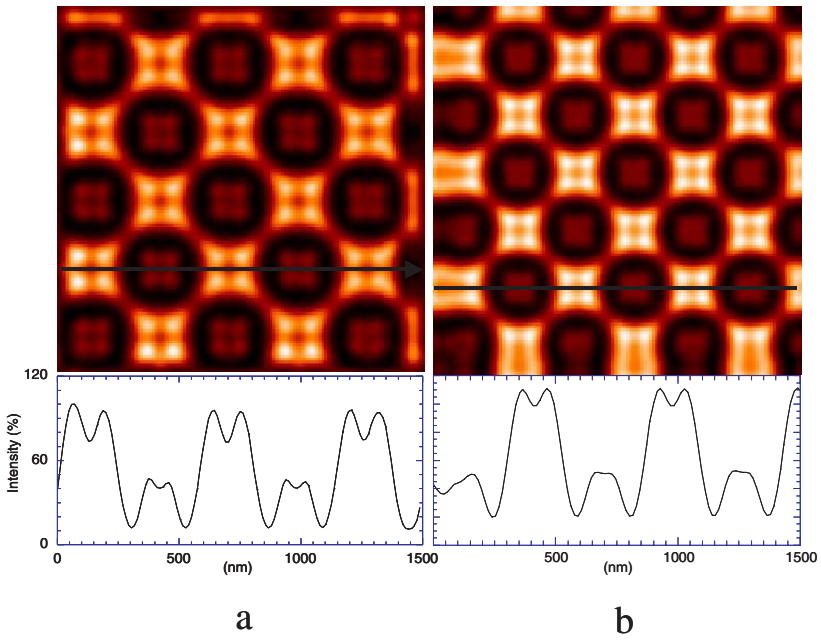

Figure 5. Comparison between the aerial diffraction pattern simulation generated by the x-ray mask pattern obtained increasing the spatial blur from the real value of 1 nm (figure 5(a)) to a spatial blur of 10 nm (figure 5(b)). In both cases a 15 μm mask–substrate gap has been used. At the bottom panel the intensity profiles along the cut line reported on the aerial diffraction patterns are reported.

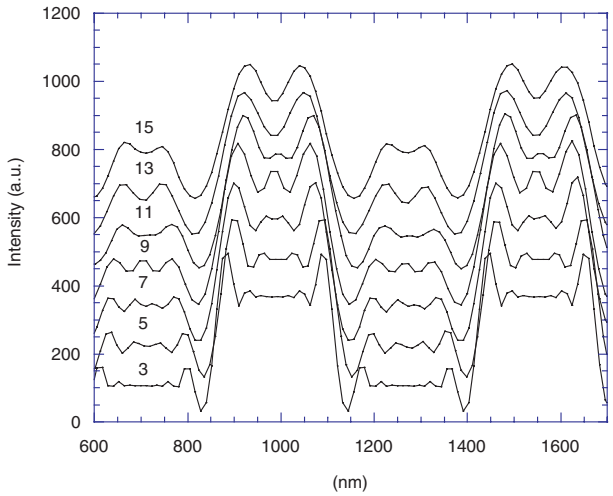

Figure 6. Comparison of intensity profiles obtained varying the mask–substrate gap from 3 to 15 μm.

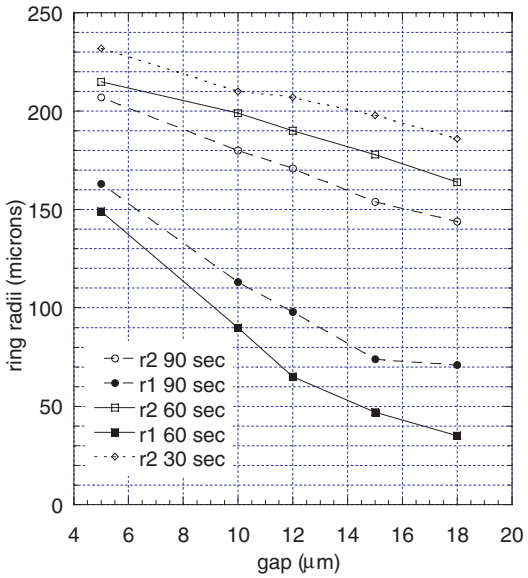

Figure 7. Internal and external radius of the two-dimensional lattice basis obtained for different mask–substrate gaps and developing times.

exposure dose and of the development time is required. This study has also been performed exploiting the part of TOOLSET devoted to resist development. The PMMA and SAL 601 resist dissolution rate [26] have been introduced in order to compute the resist development time evolution on a representative area. In figures 3(a)–(d) we have also reported the simulation of the resist structures. A good agreement with the experimental features has been obtained; as an example the square shape of the internal hole in figure 3(d) is well reproduced. It is worthwhile to note that the simulation appears to be the negative of the final patterning on the samples. This is because the final step of the sample fabrication is constituted by the etching of GaAs/AlGaAs waveguide epilayer, a process that inverts the tone of the resist pattern.

Several combinations of internal and external radii of the rings or a controlled smoothing of the squared angles can be achieved choosing the right experimental conditions. The key parameter in this case is the contrast between the absolute and local maxima (and minima) of the diffraction pattern (figure 5(b)) that is high enough (more than 20%) to guarantee the modulation of the lithographic structures. The mask–substrate gap dependence of the internal and external diameters of rings for three different development time (30, 60 and 120 s) is reported in figure 7 for PMMA resist and a dose of 3.5 J cm^{-2}. It turns out that a large range of configurations can be achieved.

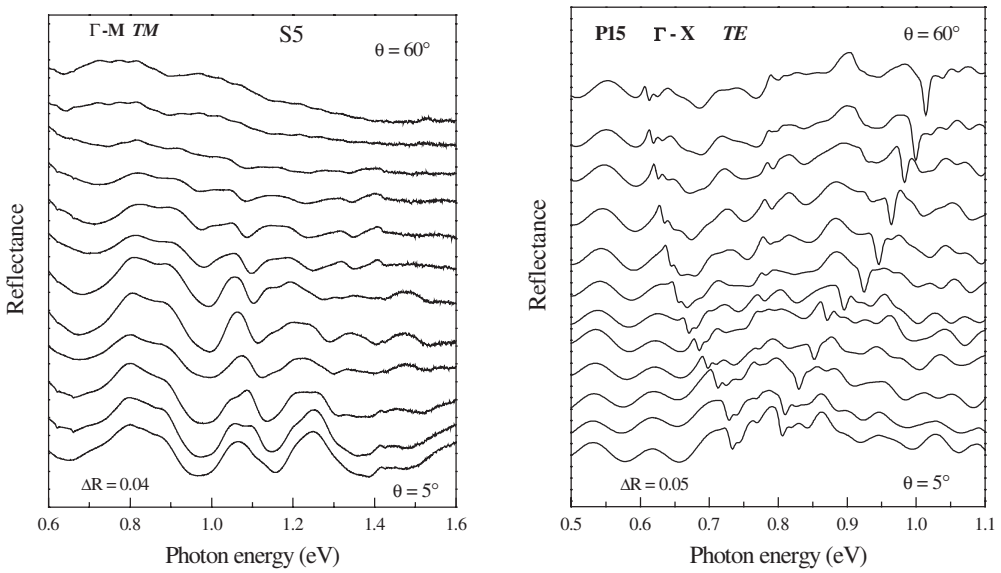

Figure 8. Experimental reflectance spectra from 5° to 60° for the S5 sample (left) and P15 sample (right) measured in the specified polarizations and directions. Curves are shifted vertically by a constant offset in order to facilitate viewing.

At 30 s no holes can be opened in the base of the lattice that, in contrast, can be obtained at 60 s. A further increase of the development time decreases the external radius and increases the internal one, resulting in a thinning of the ring walls (we are considering the resist structure; the opposite happens for the etched structure). The structures of 50 nm ring wall thickness were considered the fabrication limit of this process.

4. Optical characterization

The photonic band structure was investigated by means of the surface coupling technique proposed by Astratov *et al* [27] for a III–V PC. The method relies on the observation of sharp resonances in the reflectance spectra of collimated light incident on the surface of the PC. Variable-angle specular reflectance was measured in the range 0.25–2 eV by a Bruker IFS66 Fourier-transform spectrometer at a spectral resolution of 1 meV. The angle of incidence θ was varied in the range 5°–60° with a step of 5° and angular resolution of $\pm 1°$. Measurements were made for light incident along the Γ–X and Γ–M orientations of the samples, both in transverse electric (TE) and transverse magnetic (TM) polarizations [28][7,8].

The reflectance spectra of the S5 sample for TM polarized light incident along the Γ–M orientation and of the P15 sample for TE polarized light incident along the Γ–X orientation are shown in figure 8. As a first remark, the experimental reflectance curves show a regular interference pattern originated from the multilayer GaAs/AlGaAs waveguide structure of the sample. The interference features clearly differ from one sample to the other: this follows from the different effective refractive index of the PC slab, as determined by the dielectric fraction. Superimposed on this interference background, several features are observed which display a well defined dispersion in their energy positions with increasing angle of incidence. These resonances are due to the coupling of external radiation to guided modes of the patterned waveguide. We underline the sharpness of the resonances in the case of sample P15 as compared to S5. The experimental reflectance curves show several resonances which display a well defined dispersion in their energy positions with increasing incidence angle. The dispersion of the photonic bands can be extracted by plotting the energy positions of the resonances versus the wavevector $k = \omega \sin\theta/c$ that spans the first Brillouin zone, as shown in figure 9(a) for sample S5 and in figure 9(b) for the P15 sample. The results of a theoretical calculation reproduce all qualitative features of the photonic band dispersion with discrepancies from experimental data remaining below 0.05 eV [29].

We compare TE band sample S5, i.e. the sample obtained from a one-to-one replica of the mask, with the TE band of sample P15 i.e. with a sample characterized by a *unconventional* ring shaped unit cell and, in particular, by a high dielectric filling factor, 78%. The low dielectric fraction of the other samples (S10 and S15) gave insufficient reflection features for the analysis. The band diagram of S5 shows a PBG that opens around 1.2 eV in both polarizations over most of the Brillouin zone. The PBG is large at the Brillouin zone centre and closes only very near to the zone boundary. The photonic density of states is expected to be very low in the energy region 1.15–1.25 eV, which we may call a pseudo-gap. However, we have to notice that truly guided modes, i.e. modes whose dispersion is confined between the GaAs core and the AlGaAs dispersion lines, must be present both for TE and TM polarizations. This is not the case for S5 because the dispersion of photonic modes is strongly different for the two polarizations. The lowest bands in the guided mode region have a finite cut-off wavelength imposed by the thickness of the asymmetric waveguide. The guided modes go over smoothly into the radiative region when crossing the light line. All these features should thereafter be viewed only as quasi-guided

[7] Sample S5 and sample P15 have been already described in this reference where they were named respectively RUN3 and L2.

[8] Experiments have been always performed at standard temperature and pressure (stp).

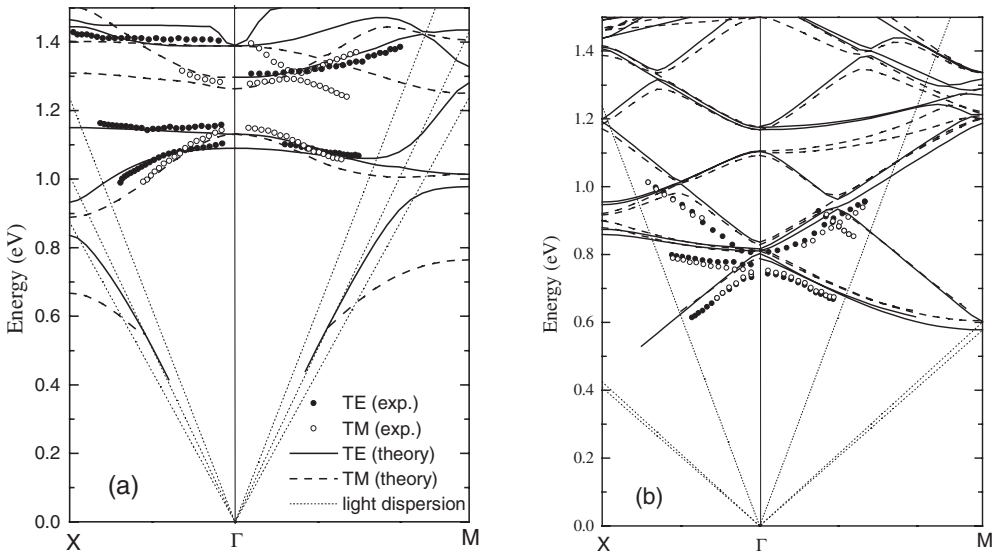

Figure 9. Photonic band structure of sample S5 (a) and of sample P15 (b) as determined from experimental reflectance spectra (symbols) and from a theoretical calculation of photonic mode dispersion (lines). Light dispersion lines in air, GaAs and AlGaAs are also reported (dotted lines).

modes and are consistent with a basis of dielectric squares and a low dielectric fraction of 28%.

The overall situation for sample P15 is rather different. The TE and TM bands are now very close and show a fairly similar dispersion. These are features typical of 'free photon' propagation in an average material. The dispersion of photonic modes is linear over most of the Brillouin zone and displays small gaps at the zone centre or edge. This is due to the high dielectric fraction of the patterning and is a further indication of free-photon-like behaviour. In both polarizations an anti-crossing of levels along the Γ–M direction around 0.9 eV is observed and is well reproduced by the theory. Actually, due to the quite high dielectric fraction of this particular sample, the system is very close to the ideal *empty lattice* or *free photon* case, where light propagation would be simply governed by an unpatterned slab waveguide with the average refractive index.

The present findings indicate that PCs with the same symmetry and the same film structure but with very different dielectric fractions show very different light guide performance. The propagation losses of photonic modes have an intrinsic component, related to out-of-plane diffraction of quasi-guided modes above the light line, and an extrinsic component arising from finite hole depth, roughness, inhomogeneities etc: all these mechanisms contribute to diffuse scattering losses. The intrinsic mechanism of diffraction arises from the non-separability of the dielectric tensor as a function of spatial coordinates, which produces a coupling of the quasi-guided modes to the external radiation field. Intrinsic diffraction losses are due to decrease with the dielectric fraction, as follows from experimental and theoretical results.

5. Conclusion

Diffraction effects on x-ray lithography have been exploited to generate a two-dimensional PC with an unconventional unit cell lattice. A high spatial degree of coherence and the precise control of the mask–substrate gap distance are the crucial parameters that allow us to generate strong modulated illumination patterns on the resist. Computer simulations have shown that even starting from a relatively simple mask made of squares on a square lattice, rhombs or four-leaf clovers can be generated. In order to avoid any complication of shape dependence we focused on the fabrication of ring and anti-ring two-dimensional PCs with or without concentric pillars or holes on an air/GaAs/AlGaAs waveguide. The size modulation of the internal ring and of the eventual central pillar has been achieved exploiting exposure dose and resist development time calibration. Wall rings down to 50 nm and central pillars of 100 nm have been realized on 4×4 mm^2 areas.

The optical characterization has shown that the fabricated two-dimensional PCs have definite optic band structures. This technique can be applied to investigate the influence of the unit cell lattice shape on the optic characteristics of the PC. In this work we focused on the influence of the filling factor. The present findings indicate that samples with very high dielectric fraction do indeed have narrow reflectance structures arising from well defined photonic modes: these modes must therefore have small radiative linewidths and low propagation losses.

Acknowledgment

This work was supported in part by INFM PAIS 2001 project '2DPHOCRY'.

References

[1] Campbell M, Sharp D N, Harrison M T, Denning R G and Turberfield A J 2000 *Nature* **404** 53
[2] Vlasov Y A, Bo Xiang-Zheng, Sturm J C and Norris D J 2001 On-chip natural assembly of silicon photonic bandgap crystals *Nature* **414** 289–93
[3] Wijnhoven J E G J and Vos W L 1998 Preparation of photonic crystals made of air spheres in titania *Science* **281** 802–4

[4] Shoji S and Kawata S 2000 Photofabrication of three-dimensional photonic crystals by multibeam laser interference into a photopolymerizable resin *Appl. Phys. Lett.* **76** 2668
[5] Bullock D L, Shih C and Margulies R S 1993 *J. Opt. Soc. Am.* B **10** 399
[6] For a review see
Krauss T F and De La Rue R M 1999 Photonic crystals in the optical regime past, present and future *Prog. Quantum Electron.* **23** 51–96
[7] Cheng C C, Scherer A, Tyan R C, Fainman Y, Witzall G and Yablonovitch E 1997 *J. Vac. Sci. Technol.* B **15** 2764–67
[8] Chow E, Lin S Y, Johnson S G, Villeneuve P R, Joannopoulos J D, Wendt J R, Vawter G A, Zubrzycki W, Hou H and Alleman A 2000 Three-dimensional control of light in a two-dimensional photonic crystal slab *Nature* **407** 983–6
[9] Painter O, Lee R K, Scherer A, Yariv A, O'Brien J D, Dapkus P D and Kim I 1999 Two-dimensional photonic band-gap defect mode laser *Science* **284** 1819–21
[10] Krauss T F and DeLa Rue R M 1996 Optical characterization of waveguide based photonic microstructures *Appl. Phys. Lett.* **68** 1613
[11] Moosburger J, Kamp M, Klopf F, Fuscher M and Forchel A 2001 Fabrication of semiconductor laser with 2D-photoniccrystal mirrors using a wet oxidized Al203-mask *Microelectron. Eng.* **57/58** 1017–21
[12] Meade R D, Brommer K D, Rappe A M and Joannopoulos J D 1991 *Phys. Rev.* B **44** 13 772–4
[13] Joannopouls J D, Villeneuve P R and Fan S 1997 *Nature* **386** 143
[14] Villeneuve P R and Piché M 1992 *Phys. Rev.* B **46** 4969–72
[15] Cassagne D, Jouanin C and Bertho D 1996 *Phys. Rev.* B **53** 7134–42
[16] Wang Rongzhou, Wang Xue-Hua, Gu Ben-Yuan and Yang Guo-Zhen 2001 *J. Appl. Phys.* **90** 4307
[17] Noda S, Yokoyama M, Imada M, Chutinan A and Mochizuki M 2001 *Science* **293** 1123
[18] Bollepalli S B, Khan M and Cerrina F 1997 Modeling image formation in layered structures, application to x-ray lithography *Proc. MSM Conf. (Tokyo,1997)*
[19] webpage http://www.elettra.trieste.it/experiments/beamlines/lilit/index.html
[20] Romanato F, Di Fabrizio E, Vaccari L, Altissimo M, Cojoc D, Businaro L and Cabrini S 2001 LILIT beamline for soft and deep x-ray lithography at Elettra *Microelectron. Eng.* **57/58** 101–7
[21] For further details on the optical layout of LILIT beam line see Di Fabrizio E, Nucara A, Gentili M and Cingolani R 1999 *Rev. Sci. Instrum.* **70** 1605
[22] Hector S D, Schattenburg M L, Anderson E H, Chu W, Wong V V and Smith H I 1992 *J. Vac. Sci. Technol.* B **10** 3164
[23] Guo J Z Y, Leonard Q, Cerrina F, Di Fabrizio E, Luciani L, Gentili M and Gerold D 1992 *J. Vac. Sci. Technol.* B **10** 3150
[24] Khan M, Mohammad L, Xiao J, Ocola L and Cerrina F 1994 *J. Vac. Sci. Technol.* B **12** 3930
[25] Khan M, Bollepalli B S and Cerrina F 1997 *CNTech Toolset User's Guide*, *University of Wisconsin—Madison Report*
[26] Khan M, Bollepalli S B and Cerrina F 1997 A semi-empirical resist dissolution model for sub-micron lithographies *Proc. MSM Conf. (Tokyo, 1997)*
[27] Astratov V N, Whittaker D M, Culshaw I S, Stevenson R M, Skolnick M S, Krauss T F and De La Rue R M 1999 *Phys. Rev.* B **60** R16 225
[28] Galli M, Agio M, Andreani L C, Atzeni L, Bajoni D, Guizzetti G, Businaro L, Di Fabrizio E, Romanato F and Passaseo A 2002 Optical properties and photonic bands of GaAs photonic crystal waveguides with tilted square lattice *Eur. Phys. J.* B **27** 79–87
[29] Andreani L C and Agio M 2002 Photonic bands and gap maps in a photonic crystal slab *IEEE J. Quantum Electron.* at press